JOURNAL OF GUIDANCE, CONTROL, AND DYNAMICS
Vol. 26, No. 4, July–August 2003

Heating and Modeling Effects in Tethered Aerocapture Missions

Paul Williams*
Royal Melbourne Institute of Technology, Melbourne, Victoria 3001, Australia
Sherrin Yeo†
General Electric Aircraft Engines, Tullamarine, Victoria 3043, Australia
and
Chris Blanksby‡
Royal Melbourne Institute of Technology, Melbourne, Victoria 3001, Australia

The influence of thermomechanical and tether flexibility effects on tethered aerocapture missions is examined. The focus of these missions is capturing a system, consisting of an orbiter and tether-connected probe, from a hyperbolic to an elliptical orbit via aerodynamic braking. Two temperature-dependent dynamic models of the tether are included: a two-dimensional, straight, massive, extensible tether model derived via Lagrange's equations and a three-dimensional lumped mass model derived via Kane's equations. The dynamics of the aerocapture maneuver are shown to be affected by tether extensibility due to the change in system rotational inertia. If not properly accounted for, this can result in non-capture. The effect of thermal variations on the dynamics of the aerocapture maneuver is shown to be influenced strongly by the thermal properties of the tether material. As a consequence, these thermal variations can decrease the viability of certain proposed tethered aerocapture missions and should be accounted for during design.

Nomenclature

A_j	=	aerodynamic area of the jth tether element
a	=	albedo coefficient for the central planet, Earth = 0.367 and Mars = 0.150
a_{IR}	=	infrared absorptivity of the tether material
a_s	=	solar absorptivity of the tether material
C_{D_j}	=	drag coefficient of the jth tether element
c_m	=	specific heat of the tether material
d_j	=	diameter of the jth tether element
EA	=	tether longitudinal stiffness
F^{drag}	=	generalized drag forces used in Kane's equations
F^g	=	generalized gravity forces used in Kane's equations
F^s	=	generalized spring forces used in Kane's equations
$\boldsymbol{F}_j$	=	drag force on jth tether element in dumbbell model
f_j	=	central planet view factor for the jth tether element
I_s	=	average solar constant at the central planet, Earth = 1372 W/m^2 and Mars = 590 W/m^2
L_s	=	nominal unstrained tether length at temperature, T_{ref}
$\mathcal{L}$	=	Lagrangian of the dumbbell tether system
l	=	total tether length
m	=	total system mass
m_1	=	mass of body 1 in dumbbell model
m_2	=	mass of body 2 in dumbbell model
n	=	number of discrete tether elements in dumbbell model
Q_j^{albedo}	=	planetary albedo flux for the jth tether element
Q_j^{drag}	=	aerodynamic heat flux for the jth tether element
Q_j^{IR}	=	infrared radiation flux for the jth tether element
Q_j^{rad}	=	radiative heat flux for the jth tether element
Q_j^{solar}	=	solar heating flux for the jth tether element
Q_{q_j}	=	generalized forces in Lagrange's equations
q_j	=	generalized coordinates used in lumped mass model
R	=	radius to the system center of mass in dumbbell model
$\boldsymbol{R}$	=	vector from the central planet to the orbiter in lumped mass model
$\boldsymbol{R}_j^{\mathrm{center}}$	=	vector from the planet to the center of jth tether element in lumped mass model
R_{Mars}	=	radius of Mars
$\boldsymbol{r}_j$	=	vector joining the $(j-1)$th lumped mass to the jth lumped mass
r_1	=	distance of m_1 from the center of mass in dumbbell model
r_2	=	distance of m_2 from the center of mass in dumbbell model
T	=	average tether temperature
T_e	=	equivalent blackbody temperature of the central planet, Earth = 288 K and Mars = 218 K
T_{ref}	=	tether reference temperature
u	=	generalized speeds used in lumped mass model
$\boldsymbol{v}_j$	=	inertial velocity of the jth lumped mass
$\boldsymbol{v}_j^{\mathrm{atm}}$	=	velocity of the atmosphere at the center of the jth tether element
x_j	=	distance to the center of the jth element from the center of mass in dumbbell model
α	=	in-plane libration angle
α_{sun}	=	position angle of the sun defined in Fig. 3
β_j	=	sun-view angle of jth tether element defined in Fig. 3
γ_j	=	tether view angle defined in Fig. 3
ε	=	emissivity of the tether material
θ	=	true anomaly of the tether system center of mass
ξ	=	coefficient of thermal expansion of the tether material
ϑ_j	=	angle of attack of the jth tether element to the flow
μ	=	gravitational constant of the central body
ρ_j	=	atmospheric density at the center of the jth tether element or mass
ρ_{tether}	=	linear density of the tether material
σ	=	Stefan–Boltzmann constant
φ_j	=	solar angle defined in Fig. 3
$\varphi_{\mathrm{shadow}}$	=	solar shadow angle defined in Fig. 3
ψ_j	=	solar zenith angle at the center of the jth tether element, $\pi - \varphi_j$

Subscripts

j	=	jth tether element

Received 18 March 2002; revision received 10 October 2002; accepted for publication 26 March 2003.

*Ph.D. Candidate, School of Aerospace, Mechanical and Manufacturing Engineering.
†Field Service Engineering.
‡Senior Research Fellow, School of Aerospace, Mechanical and Manufacturing Engineering.

o = orbiter
p = probe
t = tether

Superscript

rel = measured relative to the atmosphere

I. Introduction

THE use of tethers as an alternative to chemical propulsion has become a popular topic in the tether research community.[1,2] In particular, the use of tethers in aerocapture missions has been examined in some detail in Refs. 3–10. The tethered aerocapture scenario utilizes a system, consisting of an orbiter–tether–probe combination, on a hyperbolic orbit past a target planet. As the system approaches the target planet, the probe is lowered into the atmosphere. The aerodynamic drag forces acting on the tether and probe are designed to cause the system to be decelerated (captured) from an initial hyperbolic orbit to an elliptical orbit about the planet. As such, no chemical propellant is required to decelerate a spacecraft once it reaches the target planet on an interplanetary mission.

The fundamental nature of the dynamics of the aerocapture maneuver has been studied in detail in Refs. 3–10, but the analyses have not yet included the influence of thermal perturbations on the system. This appears to be a significant omission because temperature effects may be one of the most critical aspects of the tethered aerocapture mission. First, the tether must be able to withstand the high loads and temperatures without melting or failing.[11] Second, the thermal interactions may cause significant vibrations or changes in assumed parameters (such as length) that may be detrimental to the aerocapture maneuver. A further limitation of existing studies is that no investigation has been undertaken to assess the impact of certain modeling assumptions on the validity of the results.

The purpose of this paper is, therefore, twofold: 1) to investigate the effect of different tether modeling approaches on the dynamics of the aerocapture maneuver and 2) to investigate the effect of tether heating on the dynamics of the aerocapture maneuver. The effect of modeling has an impact on the study of the effect of tether heating, and, therefore, it is important that both of these effects are considered in isolation.

II. Review of Existing Work

Much work has already been done on the interaction of tethers with an atmosphere. The major focus of past work has been on tethered Mars missions due to the promise of future human exploration. The first detailed study of the use of tethers in the Martian atmosphere was conducted by Lorenzini et al.,[12] where the lowering of a small probe into the lower atmosphere was considered for a number of different applications. The tether was modeled with a lumped mass representation that included aerothermodynamic effects, but the orbiter was restricted to a circular orbit (maintained by a thrust force). Shortly after this, Longuski and Puig-Suari[3] and Puig-Suari and Longuski[6,8] established the feasibility of the tethered aerocapture maneuver using a nonspinning tether and also considered elliptical aerobraking maneuvers. The authors used a rigid rod model of the orbiting tether system and integrated the aerodynamic forces analytically across the system, assuming an exponential atmosphere. This work was synthesized into a study of the use of aerocapture throughout the solar system in Ref. 4, where a set of design conditions was presented that leads to a unique aerocapture design.

The effects of tether bending during the aerocapture maneuver was considered in Ref. 7, where a series of linked rigid rods was used to model the tether. This analysis was extended in Ref. 10, where the effect of longitudinal flexibility was modeled by the inclusion of a spring to connect the probe to the last rigid rod in the sequence. In Refs. 9 and 13, a more advanced flexible tether model was introduced that modeled the tether as a series of rigid rods connected by springs. Subsequently, the optimal mass problem (minimum tether mass for capture) was examined in a number of papers.[5,14,15]

In Ref. 16, Krischke et al. considered tethered assisted aerodynamic reentry of the small expendable deployer system (SEDS) using a lumped mass representation of the dynamics, including thermal interactions. The thermal variations in tethered applications have been included in various analyses, for example, Ref. 17, but the impact of these variations has not been studied extensively, particularly in applications where large thermal variations are expected. Furthermore, although previous investigations have used a variety of different tether models, the impact of different modeling techniques has not been documented. These important aspects of research into the aerocapture maneuver are the focus of this paper.

III. Tether Modeling Effects on Aerocapture Simulations

Several methods have been used to model the tether in past investigations.[18] These include 1) exact continuous models, which employ mathematical discretization during solution; 2) physically discretized models, which model the tether as a series of point masses or rigid rods connected by viscoelastic springs; 3) longitudinally flexible (massless or massive) structures; and 4) completely rigid structures that are massless or massive. The way in which the tether is modeled impacts the validity of the numerical results. It is, therefore, important to choose a model that does not neglect any essential feature of the dynamics. In this paper, two independently derived models for an aerobraking tether are numerically simulated. The first treats the tether as a massive, longitudinally flexible spring and is capable of simulating the system's orbital mechanics, in-plane librations, and longitudinal extension. The second model employs a lumped mass discretization technique that is capable of simulating the full three-dimensional dynamics of a flexible tether.

A. Tether Modeled by a Single Spring

In most tether models that only account for the first longitudinal mode of vibrations, the tether is assumed to be massless and treated as a single element. In the model presented here, tether longitudinal flexibility is modeled by a single spring, but all other effects are taken into account by discretizing the tether into a series of smaller elements. Drag forces and temperatures are calculated for each element, and the principle of virtual work is used to assess the impact of these forces on the overall dynamics. This method is similar to that used in Ref. 17.

The tether system consists of an orbiter, probe, and tether. The orbiter and probe are considered to be point masses for dynamic purposes, but are modeled as spheres in aerodynamic calculations. The tether is assumed to remain constant in mass and is modeled as a rod of uniform density at any instant of time. The equations of motion for the system are derived by the use of Lagrange's equations with the generalized coordinates shown in Fig. 1a.

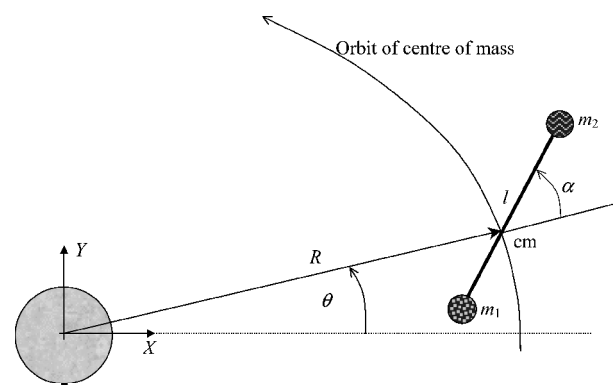

Fig. 1a Generalized coordinates used in dumbbell tether model.

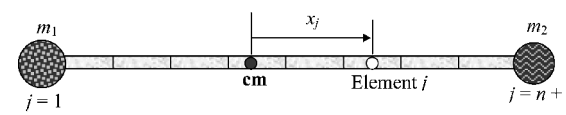

Fig. 1b Discretization of dumbbell tether for external force calculations.

The Lagrangian for the in-plane motion of an extensible massive tether is given by

$$\mathcal{L} = \frac{1}{2}m(\dot{R}^2 + R^2\dot{\theta}^2) + \frac{1}{2}m^*\dot{l}^2 + \frac{1}{2}m^*l^2(\dot{\theta}+\dot{\alpha})^2 - \frac{1}{2}\frac{EA}{L_s}[l - L_s(1+\xi\Delta T)]^2 + \frac{\mu m_1}{R_1} + \frac{\mu m_2}{R_2} - \mu\left(\frac{m_t}{l}\right)\ln\left(\frac{R_1 - r_1 + R\cos\alpha}{R_2 + r_2 + R\cos\alpha}\right) \tag{1}$$

where R, θ, α, and l are the generalized coordinates defined in Fig. 1a, EA is the tether elasticity, L_s is the nominal unstrained tether length, μ is the gravitational constant of the central planet, m_t is the tether mass, $\Delta T = T - T_{\text{ref}}$ is the average change in temperature of the tether with respect to the reference temperature T_{ref}, and

$$m^* = \left[\left(m_1 + \frac{m_t}{2}\right)\left(m_2 + \frac{m_t}{2}\right)\right] \Big/ m - \frac{m_t}{6} \tag{2}$$

$$R_1 = \sqrt{R^2 + r_1^2 - 2Rr_1\cos\alpha} \tag{3}$$

$$R_2 = \sqrt{R^2 + r_2^2 + 2Rr_2\cos\alpha} \tag{4}$$

where $r_1 = (m_2 + m_t/2)l/m$ and $r_2 = (m_1 + m_t/2)l/m$ are the distances of mass 1 and 2 from the center of mass, respectively.

The equations of motion may be derived via Lagrange's equations,

$$\frac{\mathrm{d}}{\mathrm{d}t}\left(\frac{\partial\mathcal{L}}{\partial\dot{q}_j}\right) - \frac{\partial\mathcal{L}}{\partial q_j} = Q_{q_j} \tag{5}$$

where $q_j = R, \theta, \alpha$, and l are the generalized coordinates and Q_{q_j} are generalized forces not derivable from potential functions. The full equations of motion are omitted here for the sake of brevity.

The generalized forces are due to aerodynamic drag and may be determined from the principle of virtual work.[19] Instead of calculation of the drag forces by analytical integration along the tether, a discretization approach is used, as shown in Fig. 1b. The tether is divided into n elements of length l/n. The entire system then consists of $n+2$ elements, including the orbiter and probe. The position of the center of the jth element is determined from

$$x_j = \begin{cases} -r_1 & j = 1 \text{ (mass 1)} \\ (2j - 3/2n)l - r_1 & j = 2, \ldots, n+1 \text{ (tether)} \\ r_2 & j = n+2 \text{ (mass 2)} \end{cases} \tag{6}$$

The inertial position of the center of the jth element is determined from

$$\boldsymbol{R}_j = \{R\cos\theta + x_j\cos(\theta+\alpha),\ R\sin\theta + x_j\sin(\theta+\alpha)\} \tag{7}$$

The generalized forces for the system may be determined by summation of the force contributions from each element in the system as

$$Q_{q_i} = \sum_{j=1}^{n+2} \boldsymbol{F}_j \cdot \frac{\partial \boldsymbol{R}_j}{\partial q_i} \tag{8}$$

where $\boldsymbol{F}_j$ is the drag force on the jth element, which may be calculated from Ref. 11

$$\boldsymbol{F}_j = -\tfrac{1}{2}C_{D_j}\rho_j\left|\dot{\boldsymbol{R}}_j - \boldsymbol{v}_j^{\text{atm}}\right|\left(\dot{\boldsymbol{R}}_j - \boldsymbol{v}_j^{\text{atm}}\right)A_j|\sin\vartheta_j| \tag{9}$$

where C_{D_j} is the drag coefficient of the jth element, ρ_j is the atmospheric density at the center of the jth element, $\boldsymbol{v}_j^{\text{atm}}$ is the velocity of the atmosphere (assumed to rotate with the target planet) at the center of the jth element, A_j is the aerodynamic area of the jth element, and ϑ_j is the angle of attack of the center of the jth element to the flow. Note that this equation assumes that the flow regime is free molecular, so that the drag coefficient can be assumed constant. This is the case provided the area used to calculate the drag force is the projected area of the tether normal to the flow, as in Eq. (9).

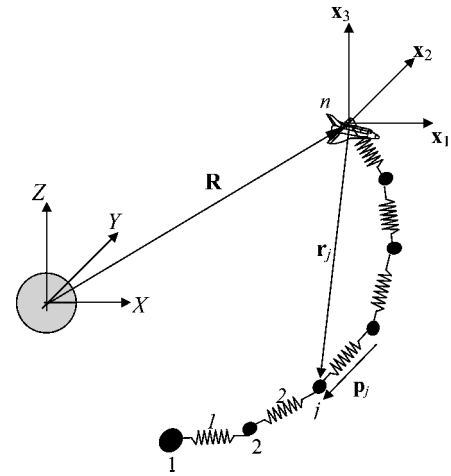

Fig. 2 Tether modeled by lumped masses.

B. Three-Dimensional Lumped Mass Tether Model

To evaluate the effects of assuming the tether is a straight body, an alternative lumped mass model of the tether has been developed. In this model, the tether is discretized into a series of lumped masses connected by massless springs, as shown in Fig. 2. The major differences between this model and the preceding one are as follows: 1) The generalized coordinates are Cartesian, not angular. 2) The model is capable of simulating in- and out-of-plane motion (three-dimensional). 3) No assumption is made as to the instantaneous distribution of mass around the mass center. This model is considered to be a more accurate representation of the physical system.

The equations of motion for the lumped mass tether system are derived by the use of Kane's equations.[20] This method of formulation allows a convenient selection of generalized coordinates and speeds for the system, ensuring both speed and accuracy.[21]

The coordinate systems employed in this model are an inertial, planet-fixed coordinate system (X, Y, Z) that is attached to the center of the target planet and a translating, nonrotating coordinate system attached to the nth mass, ($\boldsymbol{x}_1, \boldsymbol{x}_2, \boldsymbol{x}_3$). There are a total of n masses in the model, where n is the maximum number of masses allocated to represent the tether, orbiter, and probe. The masses are numbered from 1 at the probe to n at the orbiter.

The generalized coordinates are selected to improve the calculation of tension forces as

$$q_i = \boldsymbol{R}\cdot\boldsymbol{x}_i, \qquad i = 1, 2, 3 \tag{10}$$

$$\boldsymbol{p}_j = q_{3(j-1)+i}\boldsymbol{x}_i, \qquad i = 1, 2, 3;\ j = 1, \ldots, n-1 \tag{11}$$

The inertial vector to the jth mass is given by

$$\boldsymbol{R}_j = \boldsymbol{R} + \boldsymbol{r}_j, \qquad j = 1, \ldots, n-1 \tag{12}$$

where

$$\boldsymbol{r}_j = \sum_{k=j}^{n} q_{3(k-1)+i}\boldsymbol{x}_i, \qquad i = 1, 2, 3;\ j = 1, \ldots, n-1 \tag{13}$$

The generalized speeds are selected as the components of the inertial velocities of each bead

$$u_{3(j-1)+i} = \boldsymbol{v}_j\cdot\boldsymbol{x}_i, \qquad i = 1, 2, 3;\ j = 1, \ldots, n \tag{14}$$

The kinematic equations for the system are

$$\dot{q}_{3(j-1)+i} = u_{3(j-1)+i} - u_{3j+i}, \qquad j = 1, \ldots, n-1 \tag{15}$$

$$\dot{q}_{3(j-1)+i} = u_{3(j-1)+i}, \qquad j = n \tag{16}$$

Application of Kane's dynamic equations[20] gives

$$\dot{u}_{3(j-1)+i} = (1/m_j)\left[F^g_{3(j-1)+i} + F^s_{3(j-1)+i} + F^{\text{drag}}_{3(j-1)+i}\right] \qquad i = 1, 2, 3;\ j = 1, \ldots, n \tag{17}$$

where the generalized forces are defined hereafter.

Gravitational:

$$F^g_{3(j-1)+i} = -(\mu m_j/|\boldsymbol{R}_j|^3)\boldsymbol{R}_j \cdot \boldsymbol{x}_i, \quad i = 1, 2, 3;\ j = 1, \ldots, n \tag{18}$$

Spring:

$$F^s_{3(j-1)+i} = -\frac{EA}{L^s_j}\left\{1 - \frac{L^s_j[1 + \xi_j(T_j - T_{\text{ref}})]}{|\boldsymbol{p}_j|}\right\}\boldsymbol{p}_j \cdot \boldsymbol{x}_i$$

$$i = 1, 2, 3;\ j = 1 \tag{19}$$

$$F^s_{3(j-1)+i} = \frac{EA}{L^s_j}\left\{1 - \frac{L^s_j[1 + \xi_j(T_j - T_{\text{ref}})]}{|\boldsymbol{p}_j|}\right\}\boldsymbol{p}_j \cdot \boldsymbol{x}_i - \frac{EA}{L^s_{j-1}}\left\{1 - \frac{L^s_{j-1}[1 + \xi_{j-1}(T_{j-1} - T_{\text{ref}})]}{|\boldsymbol{p}_{j-1}|}\right\}\boldsymbol{p}_{j-1} \cdot \boldsymbol{x}_i$$

$$i = 1, 2, 3;\ j = 2, \ldots, n-1 \tag{20}$$

$$F^s_{3(j-1)+i} = \frac{EA}{L^s_j}\left\{1 - \frac{L^s_j[1 + \xi_j(T_j - T_{\text{ref}})]}{|\boldsymbol{p}_j|}\right\}\boldsymbol{p}_j \cdot \boldsymbol{x}_i$$

$$i = 1, 2, 3;\ j = n \tag{21}$$

Drag:

$$F^{\text{drag}}_{3(j-1)+i} = -\tfrac{1}{2}C_{D_j}\rho_j\left|\boldsymbol{v}^{\text{rel}}_j\right|\boldsymbol{v}^{\text{rel}}_j \cdot \boldsymbol{x}_i A_j$$

$$i = 1, 2, 3;\ j = 1, n \tag{22}$$

$$F^{\text{drag}}_{3(j-1)+i} = -\tfrac{1}{4}C_{D_j}\rho_j\left|\boldsymbol{v}^{\text{rel}}_j\right|\boldsymbol{v}^{\text{rel}}_j \cdot \boldsymbol{x}_i A_j(|\sin\vartheta_{j-1}| + |\sin\vartheta_j|)$$

$$i = 1, 2, 3;\ j = 2, \ldots, n-1 \tag{23}$$

where μ is the gravitational constant of the central planet, m_j is the mass of the jth mass, L^s_j is the nominal length of the jth segment at the reference temperature T_{ref}, ξ_j is the coefficient of thermal expansion of the tether material, T_j is the temperature of the jth tether element, C_{D_j} is the drag coefficient of the jth element, ρ_j is the atmospheric density at the jth element, $\boldsymbol{v}^{\text{rel}}_j$ is the velocity of the jth element relative to the atmosphere, A_j is the wetted area of the jth element, and ϑ_j is the angle of attack of the jth element to the flow.

Although the generalized coordinates do not relate specifically to orbital parameters, the orbit eccentricity of the center of mass of the system can be calculated from knowledge of the position $\boldsymbol{R}_{\text{c.m.}}$ and velocity $\boldsymbol{V}_{\text{c.m.}}$ of the center of mass at any instant of time through the eccentricity vector,

$$\boldsymbol{e} = (1/\mu)\left[V^2_{\text{c.m.}} - (\mu/R_{\text{c.m.}})\right]\boldsymbol{R}_{\text{c.m.}} - (1/\mu)(\boldsymbol{R}_{\text{c.m.}} \cdot \boldsymbol{V}_{\text{c.m.}})\boldsymbol{V}_{\text{c.m.}} \tag{24}$$

which has the orbit eccentricity as magnitude.

IV. Thermomechanical Interactions in Aerocapture Simulations

A. Tether Thermal Modeling

Several authors have modeled the effects of thermal interactions on an orbiting tether.[12,17,22–24] In this section, the equations for calculating the tether temperature in the lumped mass model (Sec. III.B.) are presented. The equations for the dumbbell model (Sec. III.A.) are simplified versions of the same equations and are not shown for the sake of brevity.

The tether is generally quite small in diameter (0.5–4 mm), and it is reasonable to assume that, at any point, the tether temperature is uniform across the cross section. The major sources of heat flux affecting the tether temperature are due to solar radiation, planetary infrared radiation, planetary albedo, aerodynamic heating, heat conduction, and self-radiation. Of the heat inputs, aerodynamic heating is the most significant in aerocapture maneuvers, and it is, therefore, prudent that this be modeled accurately.

The equation for thermal equilibrium of the jth element is given by

$$\frac{\mathrm{d}T_j}{\mathrm{d}t} = \frac{Q^{\text{solar}}_j + Q^{\text{IR}}_j + Q^{\text{albedo}}_j + Q^{\text{drag}}_j + Q^{\text{cond}}_j - Q^{\text{rad}}_j}{\rho_{\text{tether}} c_m} \tag{25}$$

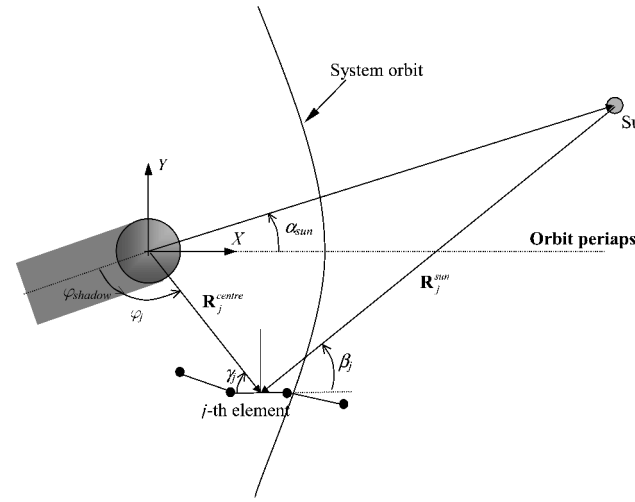

Fig. 3 Definition of parameters used in thermal calculations.

where each of the heat inputs are defined in the following subsections. The parameters used in calculating heat inputs to the system are shown in Fig. 3.

1. Solar Heating

For simplification in this analysis, the sun is assumed to lie in the tether orbital plane, and its rays are assumed to be parallel. The heat flux due to solar radiation is given by

$$Q^{\text{solar}}_j = d_j a_s I_s|\sin\beta_j|, \qquad Q^{\text{solar}}_j = 0 \qquad \text{if} \qquad |\varphi_j| \le |\varphi_{\text{shadow}}| \tag{26}$$

where d_j is the diameter of the jth tether segment, a_s is the absorptivity of the tether, I_s is the solar incident radiation at Mars (590 W/m^2), and the angles β_j, φ_j, and φ_{shadow} are defined in Fig. 3.

2. Planetary Infrared (IR) Radiation

The central planet is assumed to be a blackbody emitting infrared (IR) radiation according to

$$Q^{\text{IR}}_j = \pi d_j a_{\text{IR}} \sigma f_j T^4_e \tag{27}$$

where a_{IR} is the IR absorptivity of the tether, T_e is the equivalent blackbody temperature of Mars (218 K), and f_j is the view factor for the jth tether segment, defined in Ref. 22 as

$$f_j = (1/\pi)\left\{\sin^{-1}\left(R_{\text{Mars}}\Big/\left|\boldsymbol{R}^{\text{center}}_j\right|\right) - \sin\left[2\sin^{-1}\left(R_{\text{Mars}}\Big/\left|\boldsymbol{R}^{\text{center}}_j\right|\right)\right]\Big/2\right\} \tag{28}$$

3. Planetary Albedo

The planetary albedo radiation is determined from

$$Q^{\text{albedo}}_j = a I_s a_{\text{IR}} d_j f_j|\sin\gamma_j|\cos\psi_j$$

$$Q^{\text{albedo}}_j = 0 \qquad \text{if} \qquad \cos\psi_j < 0 \tag{29}$$

where γ_j is defined in Fig. 3 and $\psi_j = \pi - \varphi_j$ is the solar zenith angle at the center of the jth element.

4. Aerodynamic Heating

There are principally two types of heat transfer that may occur when an object impacts the atmosphere. The mechanism depends to a large extent on the nature of the airflow and the object that it is impacting. In general, for the high altitudes and small diameters of the tether system, the flow regime may be considered to be free molecular. This is the central assumption made in this paper. It means that air molecules that impact the tether do not interfere with other impacting air molecules.

The heat transferred to the tether depends on the scattering mechanism of the air molecules. Here, it is assumed that only the kinetic energy impacting normal to the tether is converted into heat, so that the heat transferred from atmospheric impact is[25]

$$Q_j^{\text{drag}} = \tfrac{1}{2}\rho_j d_j \left|\dot{\boldsymbol{R}}_j^{\text{center}} - \boldsymbol{v}_j^{\text{atm}}\right|^3 |\sin\vartheta_j| \tag{30}$$

5. Heat Conduction

Because each element in the system is considered separately, it is necessary to include the effect of heat flow between elements. In this analysis, the tether is assumed to be thermally insulated from the end bodies. The heat flow due to conduction is given by

$$Q_j^{\text{cond}} = \begin{cases} \left(A_1 \big/ L_1^s\right) k_1 (T_2 - T_1), & j = 1 \\ \left(A_j \big/ L_j^s\right) k_j (T_{j+1} + T_{j-1} - 2T_j), & j = 2, \ldots, n-2 \\ \left(A_{n-1} \big/ L_{n-1}^s\right) k_{n-1} (T_{n-2} - T_{n-1}), & j = n-1 \end{cases} \tag{31}$$

where k_j is the conductivity of the jth tether segment.

6. Radiation (Emission)

The tether radiates heat into space according to

$$Q_j^{\text{rad}} = \pi d_j \sigma \varepsilon T_j^4 \tag{32}$$

Equation (25) is integrated numerically with the equations of motion of the system to give the temperature distribution along the tether.

V. Numerical Simulation Results

To assess the impact of modeling techniques and heating effects on the aerocapture maneuver, a representative case is taken from Ref. 13. The common simulation parameters for all simulations performed in this paper are shown in Table 1. The atmospheric density calculations are performed with an exponential model, as in previous investigations.[4] Note, however, that any method or atmospheric data can be used in either of the models presented in this paper. This will be necessary to validate future aerocapture trajectories.[26]

A. Modeling Effects on Aerocapture Simulations

1. Effect of Degree of Discretization (Rigid Rod)

The degree of discretisation required for the tether to produce accurate results was examined using the rigid rod model of the tether with varying numbers of elements for drag calculations. Figure 4

Table 1 Common simulation parameters

Parameter	Values
Approach orbit parameters	
Semimajor axis	−6099.30 km
Eccentricity	1.569
Initial orbit radius to c.m.	3654.03 km
System parameters	
Orbiter mass	1000 kg
Orbiter drag coefficient	2
Orbiter area	10.5 m^2
Probe mass	1000 kg
Probe drag coefficient	1
Probe area	100 m^2
Tether mass	64.47 kg
Tether drag coefficient	2
Tether diameter	1.472 mm
Initial tether state	
α_0	280.7 deg
$\dot{\alpha}_0$	−0.01703 rad/s
L	21.046 km
Tether material properties	
E	240 GPa
Ultimate tensile strength	2.4 GPa
Melting temperature	2800 K
Atmospheric model	
Density at radius r, km, from Mars's center	$5.5 \times 10^{-8} \exp\{-[(r - 3507)/8]\}$ kg/m^3

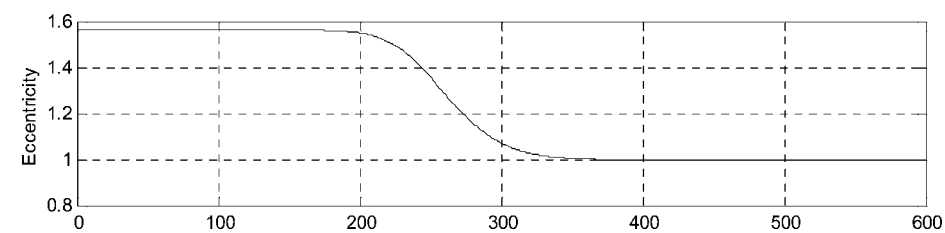

a) Orbit eccentricity of the center of mass

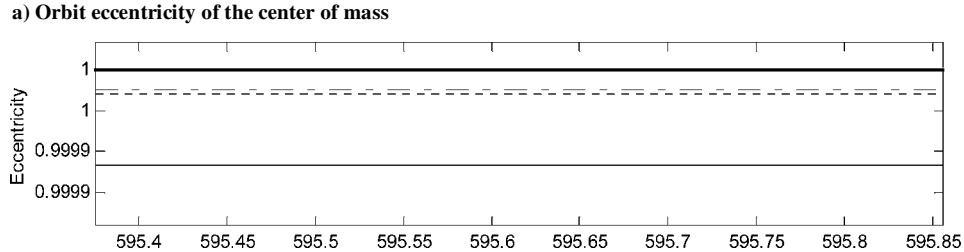

b) Final capture eccentricity (magnified)

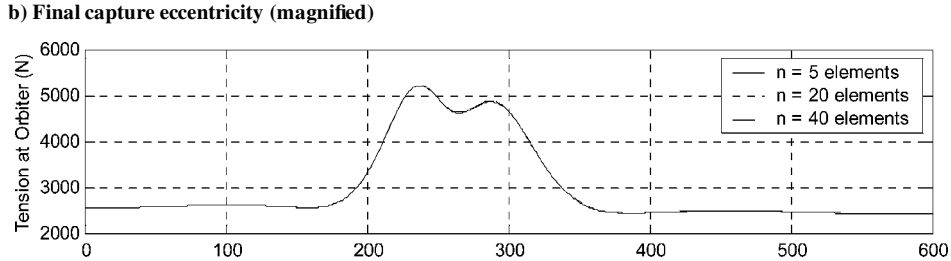

c) Tether tension at the orbiter

Fig. 4 Effect of degree of discretization on aerocapture simulations.

demonstrates that the number of elements used does not significantly impact the nature of the dynamics. There are negligible differences in the tension experienced in the tether at the orbiter end. However, the effect of the degree of discretization on the final orbit eccentricity of the system center of mass is more evident in Fig. 4b. Note that increasing the number of elements causes a very small increase in the final orbit eccentricity. This tendency is the result of improved aerodynamic drag calculations. That is, the total drag on the tether decreases as the atmospheric density calculations become more refined. Additional simulations with 100 elements show negligible change from the results where 40 elements were used. Therefore, 40 elements will be used for future simulations.

These results have important implications for application of flexible tether models, such as the lumped mass model presented in this paper. In Ref. 13, Biswell et al. criticize the use of lumped mass models in the study of tethered atmospheric missions, implying that

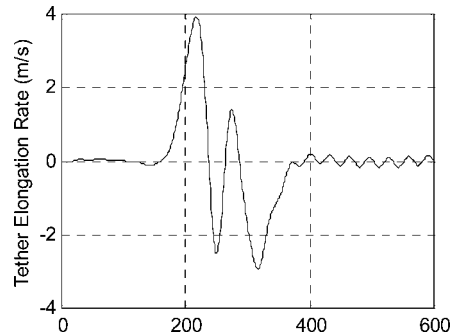

a) Rate of tether elongation

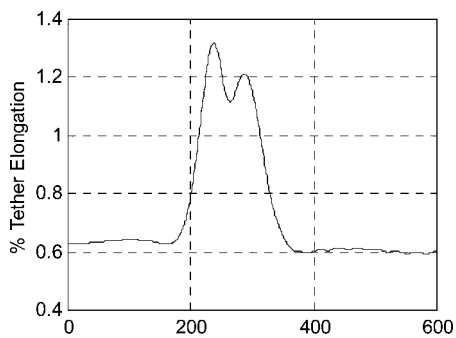

b) Relative elongation of the tether

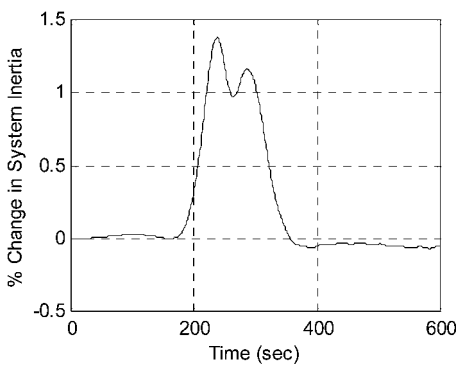

c) Relative change in system rotational inertia

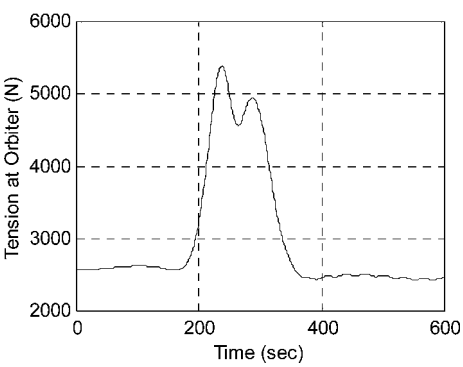

d) Tether tension at the orbiter

Fig. 5 Effect of tether extensibility on aerocapture designed with a rigid tether model.

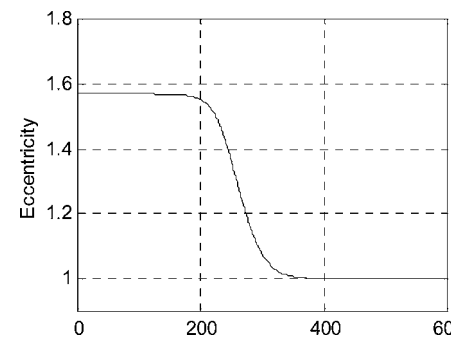

a) Orbit eccentricity of the center of mass

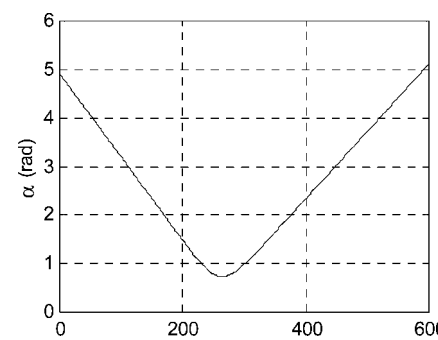

b) Tether libration angle

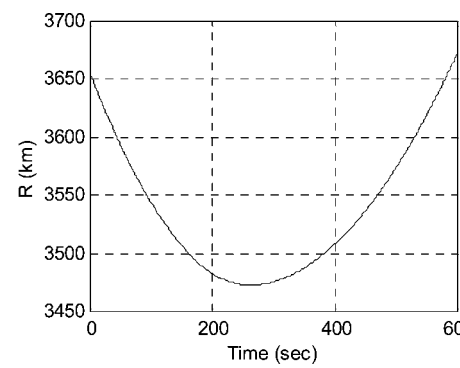

c) Orbit radius of the center of mass

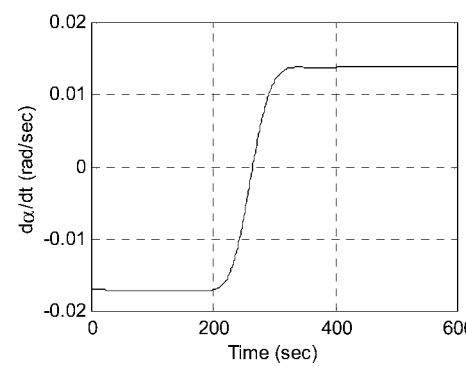

d) Tether libration rate

Fig. 6 Effect of tether extensibility on aerocapture designed with a rigid tether model.

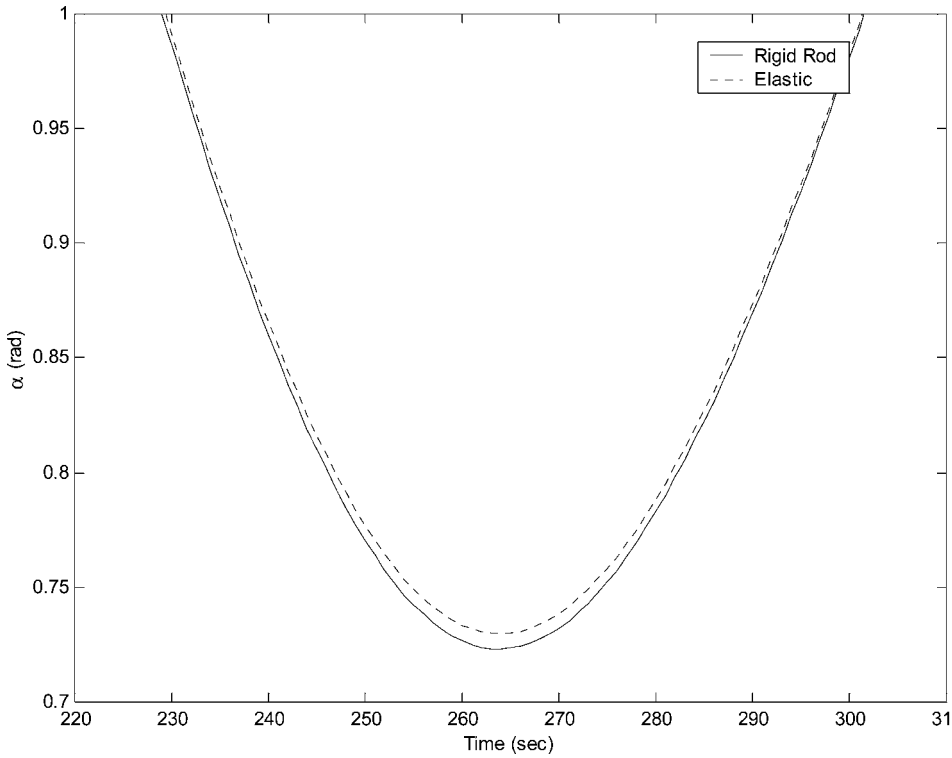

Fig. 7 Comparison of the tether libration angle during aerocapture for rigid and elastic rods.

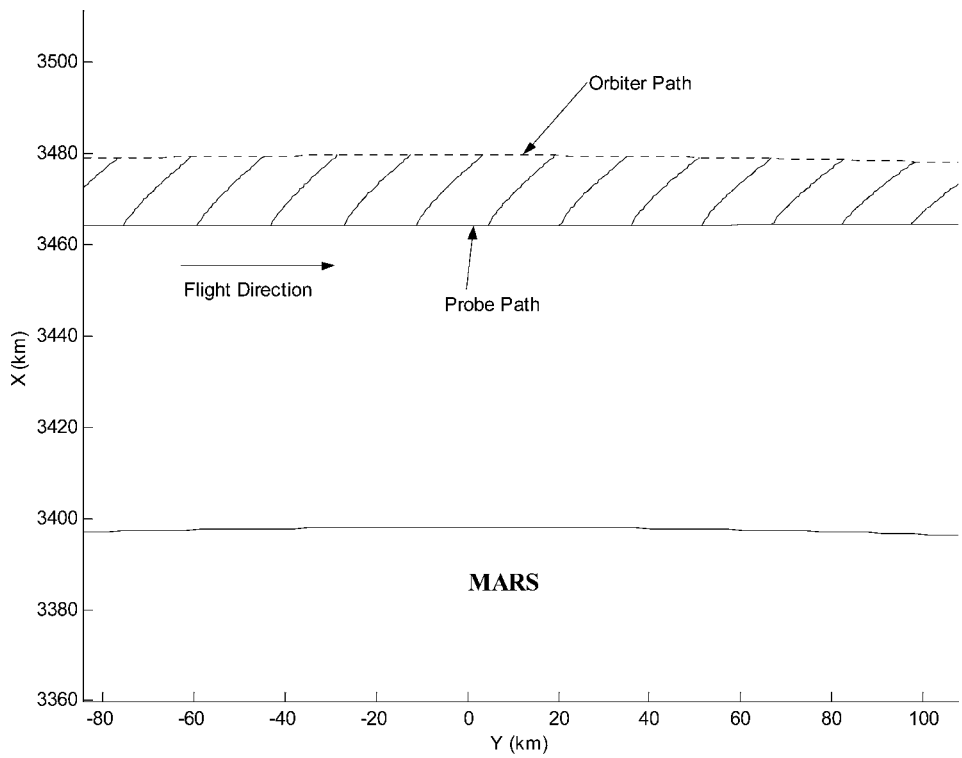

Fig. 8 Scaled plot of flexible tether during aerocapture maneuver.

no aerodynamic forces are modeled in the "gaps" between beads. They also suggest that a large degree of discretization is required to model the aerodynamic forces accurately. However, this is clearly not the case, as can be seen in the preceding results, where simulations with five elements give representative results. Although it is true that aerodynamic forces are only applied at each bead, they are calculated from knowledge of the motion of each spring segment. In addition, the preceding models are considerably simpler to derive and implement than the model presented in Ref. 13 and allow the easy inclusion of any atmospheric model.

2. *Effect of Extensible Tether*

Simulations performed with the extensible tether model allow the impact of tether extensibility on the aerocapture maneuver to be investigated. It is intuitive that a tether that is allowed to elongate may reach deeper into the atmosphere and, therefore, produce increased

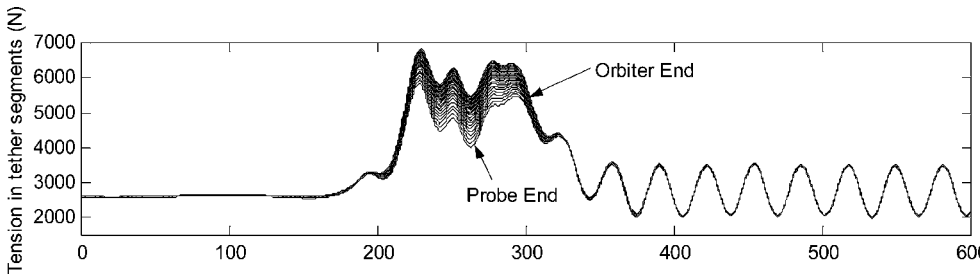

a) Tension in tether segments

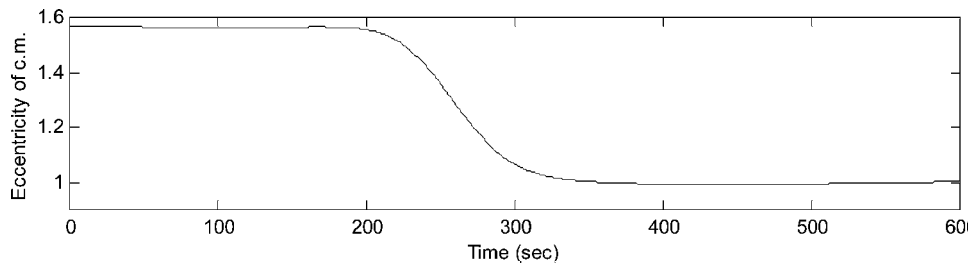

b) Eccentricity of the center of mass

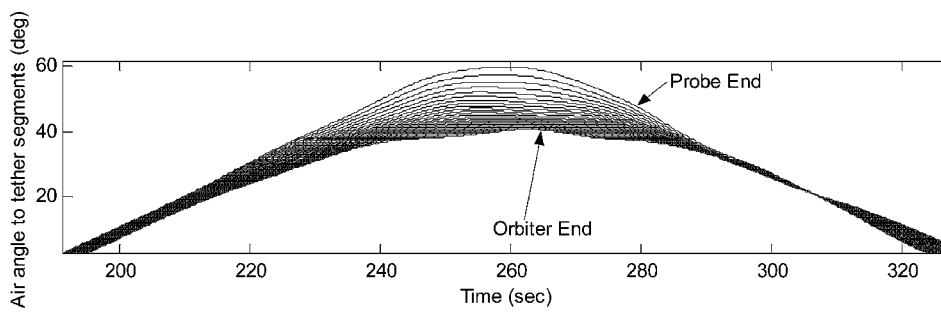

c) Angle of the incident airflow on tether

Fig. 9 Aerocapture using a flexible tether.

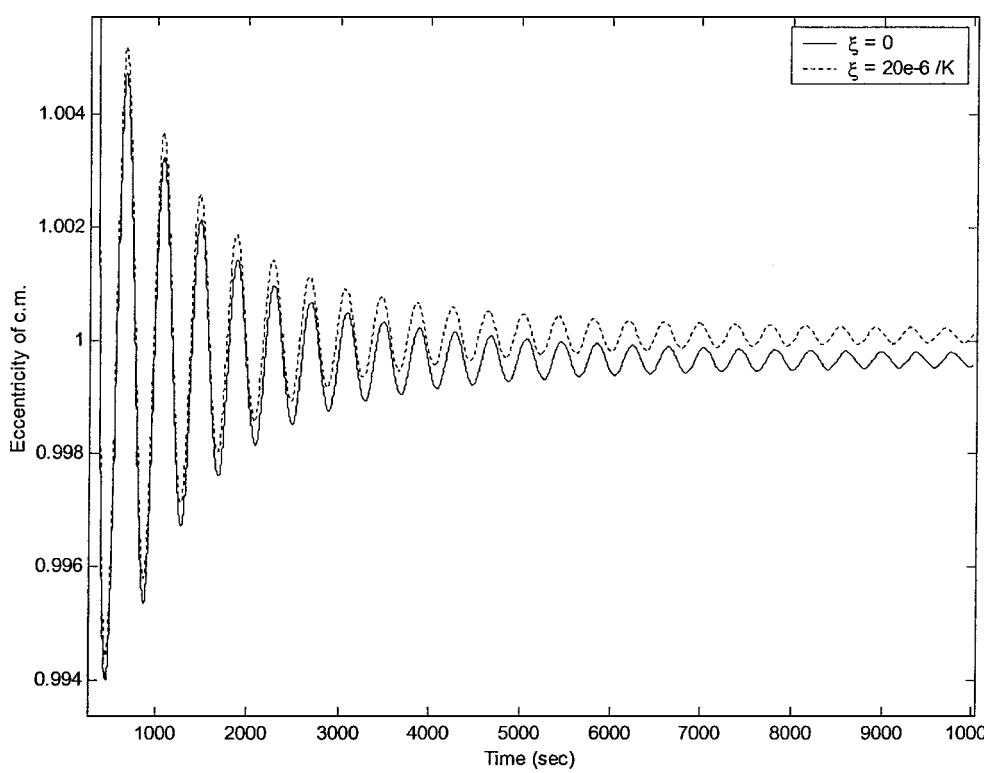

Fig. 10 Influence of heating on the final eccentricity of the center of mass for a flexible tether.

drag forces on the system. This implies that the aerocapture maneuver should be improved when an extensible tether is used. However, numerical simulations show that this is not the case. Figures 5 and 6 show numerical simulation results for an extensible tether. Whereas the overall nature of the maneuver is the same as the case of a rigid rod, the minimum eccentricity achieved by the system is increased from 0.999974 for the rigid tether to 1.00036 for an extensible tether. This counterintuitive result may be explained given that the elongation of the tether results in an increase in the system rotational inertia, as is evident in Fig. 5. This has the effect of making the tether more resistant to rotational acceleration caused by external forces. The net result is that the tether's angle of attack to the airflow is altered over time (Fig. 7), and, therefore, the total drag force acting on the system is impacted. The overall effect is a reduction in the total drag force and an increase in final orbit eccentricity. This effect can be expected to vary for different aerocapture designs.

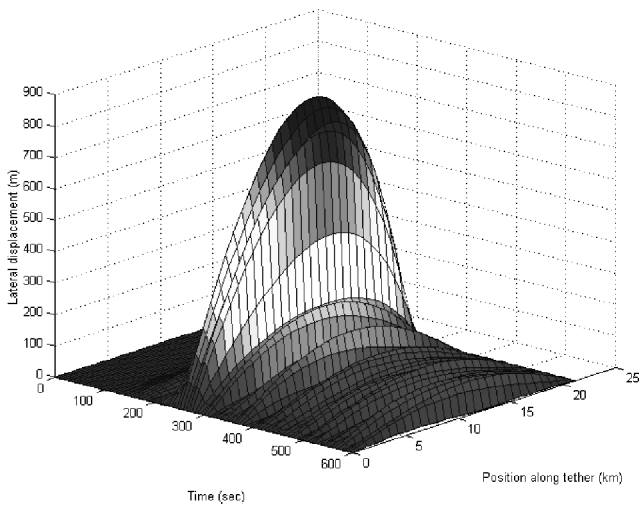

Fig. 11 Traveling wave propagation along the tether during capture.

3. Effect of Tether Bending

When the aerobraking tether impacts the atmosphere, a force is exerted normal to the tether line. This normal force causes the tether to bend, and, consequently, additional vibratory modes of the tether are excited. Simulations using the lumped mass model with 30 lumped masses show that, for this particular maneuver, the tether bending is not excessive and that the tether remains essentially straight (Fig. 8). (Note that no appreciable difference in tether dynamics was seen for more than 30 masses.) Figure 9 shows the tension distribution along the tether during the maneuver, the eccentricity of the center of mass, and the angle of the incident airflow along the tether. Figure 9 show that, when the tether impacts the atmosphere, there is a significant variation in tension along the tether (approximately 1500 N), with a maximum at the orbiter end. This can be explained by the contributions from aerodynamic drag along the tether length. Figure 9b illustrates that the most significant aspect of full tether flexibility is its influence on the orbit propagation of the center of mass. After the tether impacts the atmosphere, the trajectory of the center of mass does not remain at a constant orbit eccentricity. In fact, the orbit eccentricity initially oscillates between a hyperbolic and elliptical orbit. This is more clearly seen in Fig. 10, which also shows the effect of heating and is discussed in the next section. The variation in orbit eccentricity of the center of mass implies that the design of an aerocapture mission should include a factor of safety to ensure that the flexible system remains in an elliptical orbit after passing through the atmosphere.

Figure 11 shows the displacement of the tether perpendicular to the tether line, varying with time and the position along the tether line. Before the tether enters the atmosphere, the tether is practically straight. As could be expected, during the pass through the atmosphere, the tether takes on a very significant curvature. On leaving the atmosphere, this peak curvature dissipates quickly, but leaves a residual traveling wave, coupling longitudinal and lateral motions in the tether. This traveling wave is a very significant phenomenon and is thought to be the cause of the variation in orbit eccentricity of the center of mass. It has implications for both the viability of a particular capture scenario and for postcapture tether control.

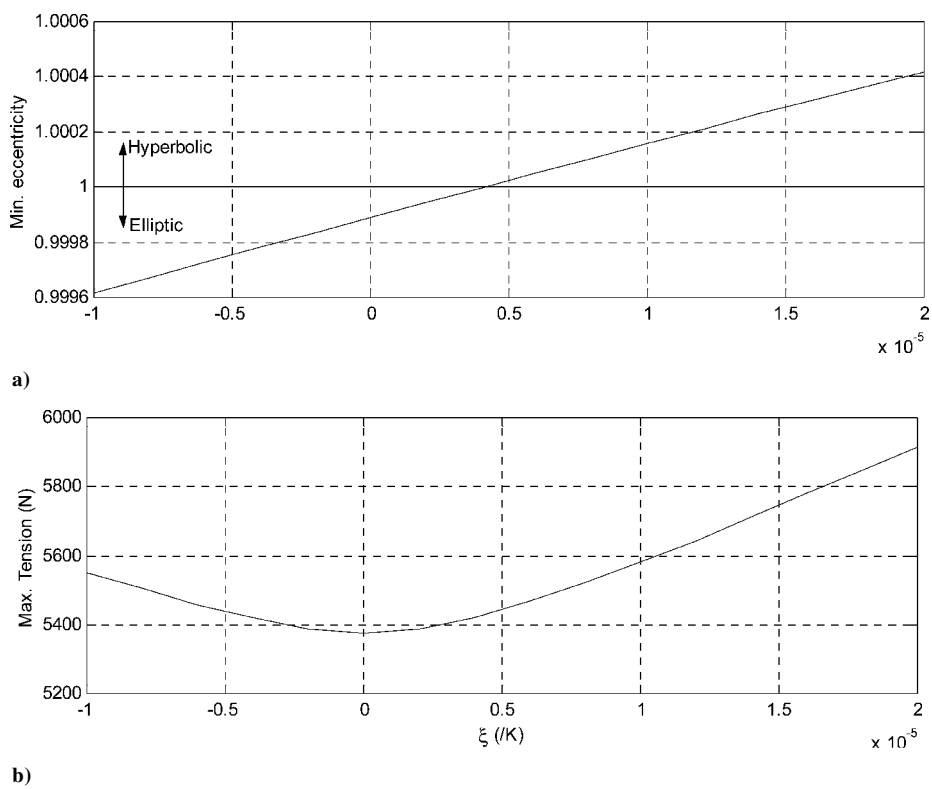

Fig. 12 Influence of tether heating on the aerocapture maneuver, showing the effect of the coefficient of thermal expansion on a) minimum achievable eccentricity and b) maximum tether tension.

Table 2 Tether thermal properties

Parameter	Value
a_s	0.5
a_{IR}	0.5
ε	0.8
k	250
c_m	700 J/(kg · K)

B. Thermomechanical Interactions During Aerocapture

The effect of tether heating on the aerocapture maneuver has two major implications. First, it must be assured that the tether material can withstand the intense heat expected during the braking maneuver. Second, the effect of thermal strains on the tether dynamics may be detrimental if the tether becomes slack at any time. To study the effect of thermal variations on the extensible system, the initial radius to the center of mass is altered slightly to 3654.4 km to ensure that the extensible tether with no thermal variations is captured.

The thermal effect on the system strongly depends on the thermal properties of the tether material. Therefore, certain parameters must be chosen carefully for a particular design. In general, the material absorptivity and emissivity are dependent on the surface texture of the material and can be controlled by coating the tether. The specific heat and coefficient of thermal expansion are material dependent. In this section, the values shown in Table 2 are adopted, and the sun is assumed to be aligned with the orbit periapsis.

The influence of the coefficient of thermal expansion on the dynamics of the capture maneuver was studied for a range of values of ξ from $-1e{-}5$ to $2e{-}5$. These are representative values for most tether materials.[11] The impact of the thermal variations on the minimum achievable eccentricity and maximum tether tension are summarized in Fig. 12. These results suggest that, for this particular maneuver, the capture eccentricity is linearly dependent on the coefficient of thermal expansion, whereas the maximum tether tension has an approximate quadratic dependence. Negative coefficients of thermal expansion imply that the tether contracts with an increase in temperature, whereas positive coefficients imply tether elongation. The results suggest that an increase in the coefficient of thermal expansion of the tether material leads to a subsequent decrease in the viability of the capture maneuver. This effect is most likely explained by the increase in system inertia with respect to the thermally unaffected system (Fig. 13).

The temperature distribution along the tether, as well as the magnitude of the heating rates due to the different sources, are shown in Fig. 14. This shows that in aerobraking maneuvers, the heating rate due to collision with the atmosphere is by far the greatest heat input. This is well matched, however, with the heat outflux from the tether due to self-radiation. This explains why the temperature decreases so rapidly after passing through the atmosphere. The least significant heating rate is that of conduction, which suggests that it is reasonable to omit this from the thermal analysis, as done by Kalaghan et al.[22] The variation in heat input due to solar radiation is due to the tether's rotation in the plane of the sun. It is, therefore, fair to conclude that the most important parameters to consider when designing a tether for aerobraking applications are the coefficient of thermal expansion and the thermal emissivity of the tether.

The tether thermal emissivity has a significant impact on the maximum temperature experienced by the tether, as shown in Fig. 15c. It is evident that the greater the emissivity of the tether, the less significant the thermal variations due to aerobraking will be on the system. A higher emissivity is preferable in terms of the likely impact on the capture eccentricity and for protection of the tether material. Because the tether thermal properties have an impact on the aerocapture maneuver, it is important to choose these carefully for a particular design, to ensure the survivability of the tether and feasibility of the capture scenario.

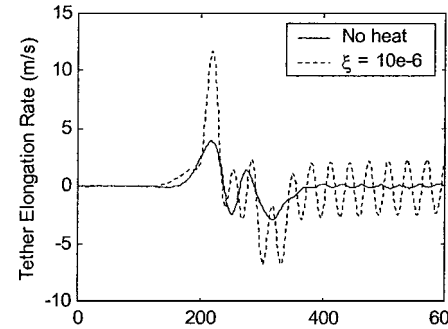

a) Tether elongation rate

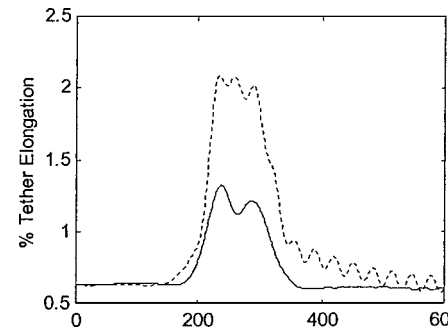

b) Relative change in tether elongation

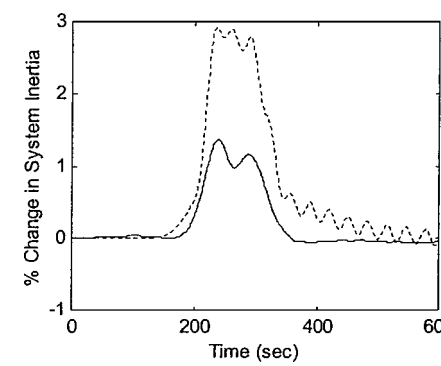

c) Relative change in system inertia

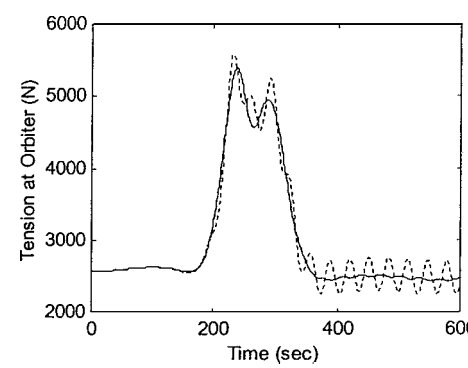

d) Tether tension

Fig. 13 Effect of tether heating on longitudinal dynamics.

The combination of tether heating and tether flexibility does not alter the preceding observations. Figure 10 shows the evolution of the eccentricity of the center of mass after the capture maneuver for a flexible tether. Initially, the center of mass oscillates between an elliptical and hyperbolic orbit. This oscillation decays over time. The case where no thermal variations are included shows that the eccentricity settles to below 1.0, but the case with thermal variations shows that the system does not remain captured.

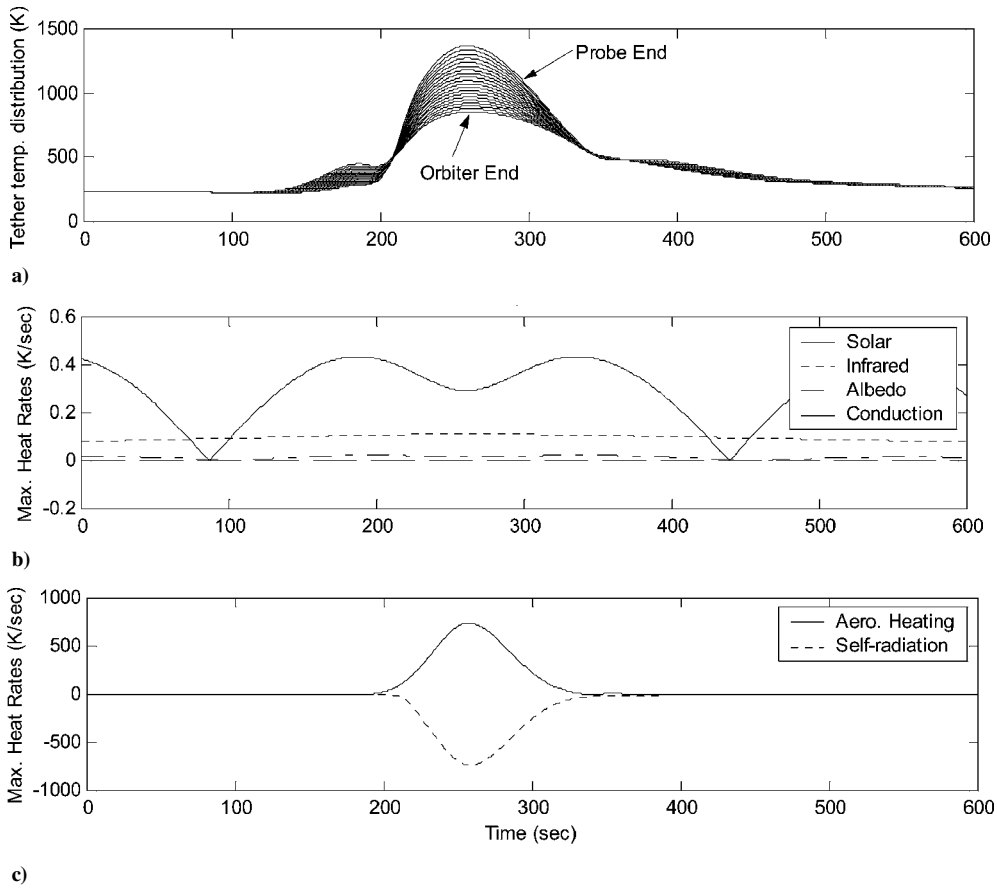

Fig. 14 Tether heating during aerocapture: a) temperature distribution along the tether; b) maximum heating rates due to solar, IR, albedo, and conduction at probe end; and c) maximum heating rates due to aerodynamic heating and self-radiation at probe end.

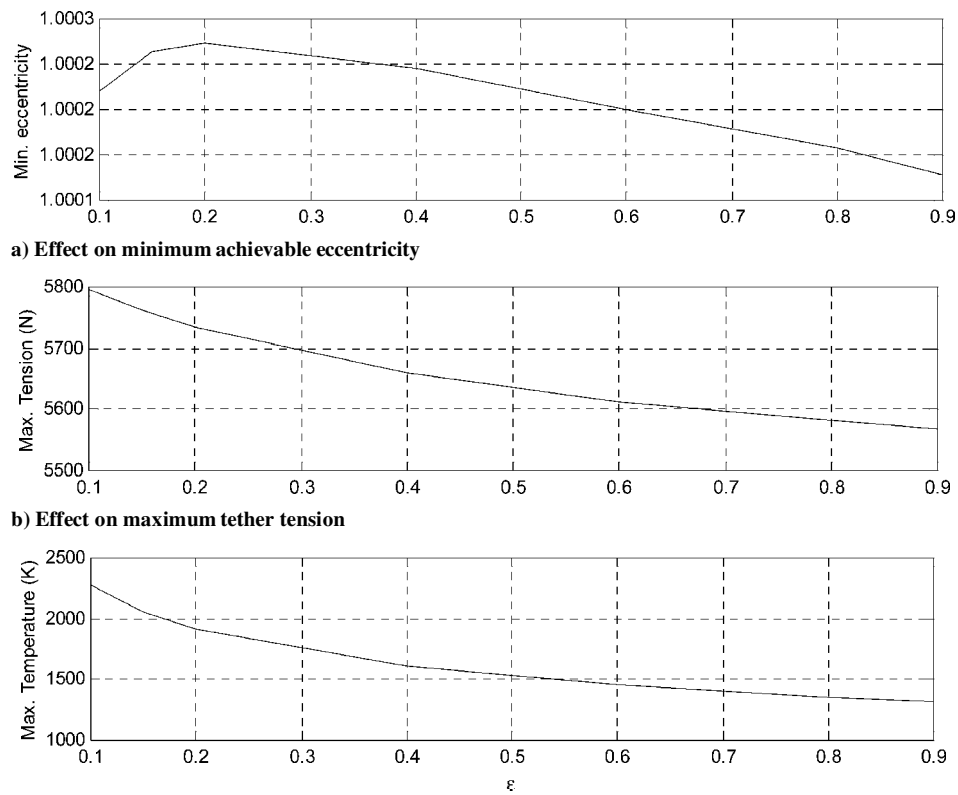

Fig. 15 Influence of tether emissivity on aerocapture ($\xi = 10e-6$).

VI. Conclusions

The dynamic interactions of tether temperature caused by aerodynamic heating has been studied with two temperature-dependent dynamic models of the tether: a two-dimensional, straight, massive, extensible tether model and a three-dimensional lumped mass model. Investigations with these two models showed that tether extensional flexibility, tether curvature, and aerodynamic heating all have a significant effect on the dynamics of the tether during aerocapture that can, in some instances, cause planetary capture to fail. The most critical parameters in the thermal analysis have been shown to be the coefficient of thermal expansion and the thermal emissivity of the tether. Although the coefficient of thermal expansion is fixed by the choice of material, the emissivity of the tether can be adjusted by coating the tether surface. The thermal variations in the system have been shown to impact the system properties, such as tether length and rotational inertia, and that these, in turn, impact the success of the aerocapture maneuver. It may, therefore, be concluded that the aerocapture maneuver should be designed with the tether thermal properties in mind, to ensure the successful application of the technology.

References

[1]Bekey, I., "Tethering a New Technique for Payload Deployment," *Aerospace America*, Vol. 35, No. 3, 1997, pp. 36–40.

[2]Hoyt, R. P., "Commercial Development of a Tether Transport System," AIAA Paper 2000-3842, June 2000.

[3]Longuski, J. M., and Puig-Suari, J., "Hyperbolic Aerocapture and Elliptic Orbit Transfer with Tethers," International Astronautical Federation, Paper IAF-91-339, Oct. 1991.

[4]Longuski, J. M., Puig-Suari, J., and Mechalas, J., "Aerobraking Tethers for the Exploration of the Solar System," *Acta Astronautica*, Vol. 35, Nos. 2–3, 1995, pp. 205–214.

[5]Longuski, J. M., Puig-Suari, J., Tsiotras, P., and Tragesser, S., "Optimal Mass for Aerobraking Tethers," *Acta Astronautica*, Vol. 35, No. 8, 1995, pp. 489–500.

[6]Puig-Suari, J., and Longuski, J. M., "Modeling and Analysis of Orbiting Tethers in an Atmosphere," *Acta Astronautica*, Vol. 25, No. 11, 1991, pp. 679–686.

[7]Puig-Suari, J., and Longuski, J. M., "Aerocapture with a Flexible Tether," *AIAA/AAS Astrodynamics Conference*, AIAA, Washington, DC, 1992, pp. 564–578.

[8]Puig-Suari, J., and Longuski, J. M., "Analysis of Aerocapture with Tethers," *Proceedings of the AAS/AIAA Astrodynamics Conference*, AIAA, Washington, DC, 1991, pp. 2487–2501.

[9]Puig-Suari, J., Longuski, J. M., and Tragesser, S. G., "Three Dimensional Hinged-Rod Model for Flexible-Elastic Aerobraking Tethers," *Proceedings of the AAS/AIAA Astrodynamics Conference*, AIAA, Washington, DC, 1993, pp. 755–774.

[10]Puig-Suari, J., Longuski, J. M., and Tragesser, S. G., "Aerocapture with a Flexible Tether," *Journal of Guidance, Control, and Dynamics*, Vol. 18, No. 6, 1995, pp. 1305–1312.

[11]Beletsky, V. V., and Levin, E. M., "Dynamics of Space Tether Systems," *Advances in the Astronautical Sciences*, Vol. 83, Univelt, San Diego, CA, 1993, Chap. 4.

[12]Lorenzini, E. C., Grossi, M. D., and Cosmo, M., "Low Altitude Tethered Mars Probe," *Acta Astronautica*, Vol. 21, No. 1, 1990, pp. 1–12.

[13]Biswell, B. L., Puig-Suari, J., Longuski, J. M., and Tragesser, S. G., "Three-Dimensional Hinged-Rod Model for Elastic Aerobraking Tethers," *Journal of Guidance, Control, and Dynamics*, Vol. 21, No. 2, 1998, pp. 286–295.

[14]Tragesser, S. G., Longuski, J. M., Puig-Suari, J., and Mechalas, J. P., "Analysis of the Optimal Mass Problem for Aerobraking Tethers," *AIAA/AAS Astrodynamics Conference*, AIAA, Washington, DC, 1994, pp. 321–329.

[15]Tragesser, S. G., Longuski, J. M., and Puig-Suari, J., "A General Approach to Aerobraking Tether Design," *Proceedings of the AAS/AIAA Astrodynamics Conference*, AIAA, Washington, DC, 1995, pp. 849–868.

[16]Krischke, M., Lorenzini, E. C., and Sabath, D., "A Hypersonic Parachute for Low-Temperature Reentry," *Acta Astronautica*, Vol. 36, No. 5, 1995, pp. 271–278.

[17]Lanoix, E. L. M., Misra, A. K., Modi, V. J., and Jablonski, A., "A Mathematical Model for Long Term Orbit and Attitude Propagation of Tethered Satellite Systems," International Astronautical Congress, Paper IAF-98-A.7.04, Sept.–Oct. 1998.

[18]Misra, A. K., and Modi, V. J., "A Survey on the Dynamics and Control of Tethered Satellite Systems," *Advances in the Astronautical Sciences*, Vol. 62, Univelt, San Diego, CA, 1987, pp. 667–719.

[19]Fowles, G. R., and Cassidy, G. L., *Analytical Mechanics*, 6th ed., Saunders College Publishing, Orlando, FL, 1999, pp. 421–425.

[20]Kane, T. R., Linkins, P. W., and Levinson, D. A., *Spacecraft Dynamics*, McGraw–Hill, New York, 1983, Chap. 4.

[21]Blanksby, C., "Non-Linear Modelling of Space Tethers and Application to Deployment, Retrieval, and Electrodynamic Operations," *Proceedings of the EMAC 2000*, Inst. of Engineers Australia, Melbourne, VIC, Australia, 2000, pp. 63–66.

[22]Kalaghan, P. M., Arnold, D. A., Colombo, G., Grossi, M. D., Kirschner, L. R., and Orringer, O., "Study of the Dynamics of a Tethered Satellite System (Skyhook)," Final Report, Contract NAS8-32199, Smithsonian Inst. Astrophysical Observatory, Cambridge, MA, 1978.

[23]Cosmo, M. L., and Lorenzini, E. C., *Tethers in Space Handbook*, 2nd ed., Smithsonian Inst. Astrophysical Observatory, Cambridge, MA, 1989.

[24]Parisse, M., "Thermomechanical Interactions in a Low Earth Orbit Tether," International Astronautical Congress, Paper IAF-00-A.3.09, Oct. 2000.

[25]Colombo, G., Gaposchkin, E. M., Grossi, M. D., and Weiffenbach, G. C., "The 'Skyhook': A Shuttle-Borne Tool for Low-Orbital-Altitude Research," *Meccanica, March* 1975, pp. 3–20.

[26]Dornheim, M. A., "Mars Atmosphere Thicker Than Expected," *Aviation Week and Space Technology*, Vol. 147, No. 13, 1997, pp. 36, 37.